Gravity Surface Wave Bifurcation in a Highly Turbulent Swirling Flow

Michael Baumer
University of Chicago and University of Chile-Santiago, FCFM

September 17, 2010

Contents

1 Introduction

Taylor-Couette flow has been the subject of many investigations in the field of fluid dynamics. The setup consists of a cylindrical tank of radius a with a concentric cylindrical rod of radius a^* mounted in the center of the tank. Then, the rod is then made to rotate at angular frequency ω. Strictly speaking, Taylor-Couette flow refers to systems where fluid fills the gap between the cylinders entirely. In our setup, we borrow the basic geometry of Taylor-Couette flow but to leave the fluid with a free surface, the volume between the rod and the interior tank wall is filled with water up to a height b. A basic diagram of the apparatus is shown below.

In his seminal work, Taylor argues that the cylindrical flow induced by the spinning interior rod remains laminar below some critical value [1]. For high rotation rates (high

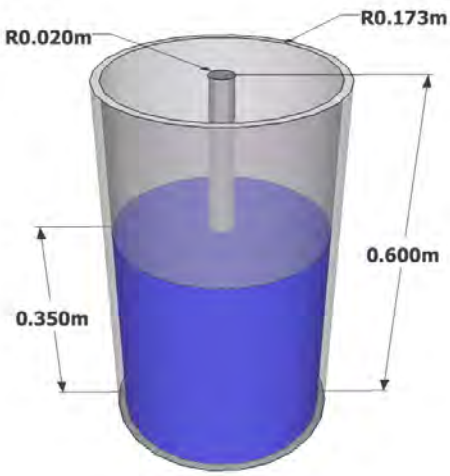

Figure 1: The main mechanical components of the system

Reynolds numbers), instabilities dominate and turbulent flow is established. In this experiment, I investigated a free-surface gravity wave bifurcation in the large-separation regime, that is, where $a - a^*$ is large. In our system, $a = 17.2\ cm$ and $a^* = 1.98\ cm$, giving us a separation of $a - a^* = 15.2\ cm$.

2 Surface Gravity Wave

The phenomenon of interest in the study of Taylor-Couette flows is a gravity wave that arises in the system as a bifurcation above a critical rotation frequency. At all rotation speeds, centrifugal force causes the rotating water to move away from the spinning rod, establishing the 'base state' that precedes any bifurcation. This state is characterized by a symmetrical, non-precessing vortex.

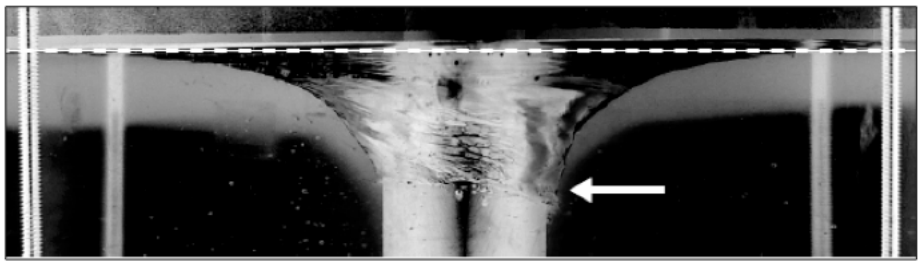

Figure 2: The 'base state' of Taylor-Couette flow. The slight asymmetry seen in this photo appears to undergo precession but time-averages to zero.

When bifurcation occurs, a gravity wave appears on the surface of the water and precesses around the axis of the tank with an amplitude that depends chiefly on the speed of the

rotating rod in the center of the tank. The main goal of this project was to use an improved apparatus to better locate the critical region where bifurcation begins. The following section describes how I detected this bifurcation and measured the properties of the resulting wave.

Figure 3: The Taylor-Couette Gravity Wave

3 Measurements

To measure the flow of water in our system and detect the Taylor-Couette gravity wave, we used a capacitive height sensor that consists of a copper wire covered with a thin layer of dielectric material. This allows the wire to function as a variable capacitor, because the water is a conductor compared to the dielectric cover. If we let a be the radius of the wire, b be the outer radius of the dielectric, and h be the height of the water, we can see that the resulting capacitance is directly proportional to the height of the water, since by simple application of Gauss' Law:

$$E = \frac{Q/h}{2\pi r\epsilon} \cdot \hat{r} \tag{1}$$

$$V = \int_a^b \frac{Q/h}{2\pi\epsilon} \cdot \frac{1}{r} \cdot dr \tag{2}$$

$$C = \frac{2\pi\epsilon}{\ln(b/a)} \cdot h \tag{3}$$

Therefore, our sensor turns the varying height of the water into a variable capacitor, whose capacitance is directly proportional to the height of the water in the tank. To extract useful information from this sensor, I attached it to the following resonant circuit:

Since the fixed capacitor and the measured capacitance from the sensor are in parallel, let's call their total capacitance $C + \Delta C$ and consider the complex impedance vector and its phase:

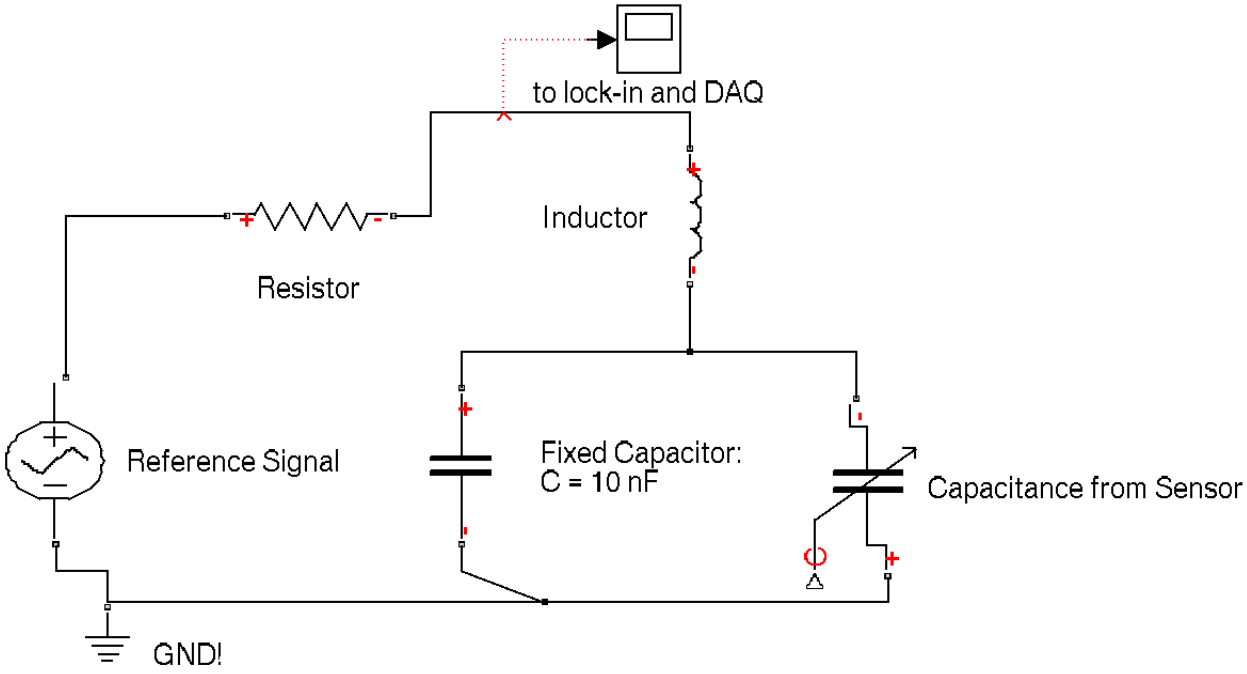

Figure 4: Resonant Circuit Diagram

$$\vec{Z} = \vec{Z_R} + \vec{Z_L} + \vec{Z_C} \tag{4}$$

$$\vec{Z} = R + i\left(\omega L - \frac{1}{\omega(C + \Delta C)}\right) \tag{5}$$

$$\phi = \arctan\left(\frac{\omega L - 1/\omega(C + \Delta C)}{R}\right) \tag{6}$$

If we assume that ϕ is small (and it is when the circuit is driven near its resonance), we can Taylor expand arctangent to get

$$\phi = \frac{\omega L - 1/\omega(C + \Delta C)}{R} = \frac{\omega L - 1/\omega C(1 + \Delta C/C)}{R} \tag{7}$$

Since $\omega L/R$ and $-1/R\omega C$ are constant, we can ignore them, since we are only concerned with how ϕ varies with ΔC. Then, since the amount that a wave amplitude could change the variable capacitance of the sensor is much smaller than the fixed capacitance of the circuit, we can Taylor expand again and obtain

$$\phi \propto \frac{-1}{R\omega C} \cdot \frac{1}{1 + \Delta C/C} \tag{8}$$

$$\phi \propto \frac{1}{R\omega C} \cdot \Delta C/C \tag{9}$$

$$\phi \propto \Delta C \propto h \tag{10}$$

Since phase is directly proportional to height, we can use a lock-in amplifier to isolate our sensor's signal from the reference signal and collect height data by reading the phase from the lock-in with an NI ADC and a computer.

4 Mechanical Hardware: Problems and Solutions

At the beginning of this project, there were several mechanical issues that were preventing the collection of reliable data. A critical mechanical component of the wave tank is a seal at the bottom of the rotating rod that protects the lower bearings from the water in the tank. At the beginning of the project, the tank had a custom-fabricated rigid graphite-teflon seal. While there was no problem with rotational friction and heat, the rigidity of the ring prevented the formation of a good seal, causing water to enter the bearings and cause destructive oxidation.

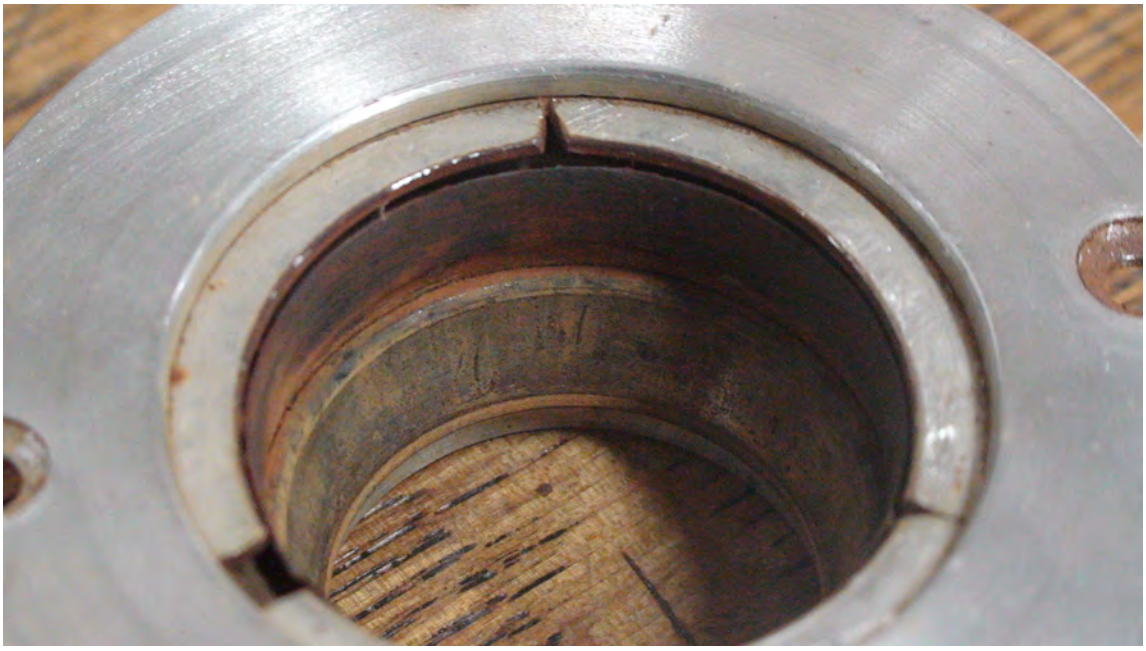

Figure 5: Interior base containing the graphite-teflon seal and rusted bearings after a trial run.

Next I modified the diameter of the lower part of the rod to fit commercial specifications for circular seals so that we could purchase and use commercial-grade seals. At first, this

change seemed to improve the performance of the lower seal and bearings. However, the first seal I tried was made of a low-quality material called *nitrilo*, and the result was that after running for a few hours, the heat produced by friction began to degrade the seal and tear small fragments off the inner lip of the seal. These fragments entered the water in the tank, got stuck on the capacitive sensor, and caused the sensor to give faulty data.

Also, as the seal released more fragments, the quality of the seal degraded, eventually allowing water into the bearings and causing rust again.

Figure 6: At left, the *nitrilo* seal before use. At right and after use, the degradation of the sealing (upper) lip is clear.

At this point, I did not know that *nitrilo* was a sub-optimal material, and I thought the problems might have been occurring because the bearings and seal were fitted poorly in their base. Therefore, I sent the cage containing the tank to the machine shop to have the top face removed. This way, I would be able to attach the base containing the bearings and seal to the bottom of the rod carefully outside the tank, checking that the filter and bearings were well-seated, put the rod and base together into the tank, and then place the lid on top. The top face remained re-attachable to the rest of the cage via bolts with pressure washers, to prevent unnecessary vibration. However, this failed to solve the problems of excessive heat, the failure of the seal, and the destruction of the bearings. Similarly, trying to use machine oil instead of grease as lubrication only made the temperature problems worse.

To solve these problems, I found a new material, called *fluoroelastómero*, for use in the seal. This material, according to the technical manual of Reténes DBH, an Argentinian company that manufactures these circular seals can withstand temperatures of up to $204\,^{\circ}C$, and is praised for its performance with water and its abrasion resistance [2].

I also found a new bearing and seal grease to replace the dirty 40 year-old grease I had previously been using. Together, these changes greatly improved the performance of the system, and allowed me to finally begin collecting reliable data.

In fact, the performance enhancements worked so well that the main cause of temperature change in the system became changes in the temperature of the room. This can be seen in the graph above, since the first half of the runs occurred in the afternoon and evening, as the room was heating up, and the second half occurred in the night and early morning, when the room was cooling down. With the new setup, 16 hour ramps ran with temperature changes of only one or two degrees, small enough to begin collecting meaningful data.

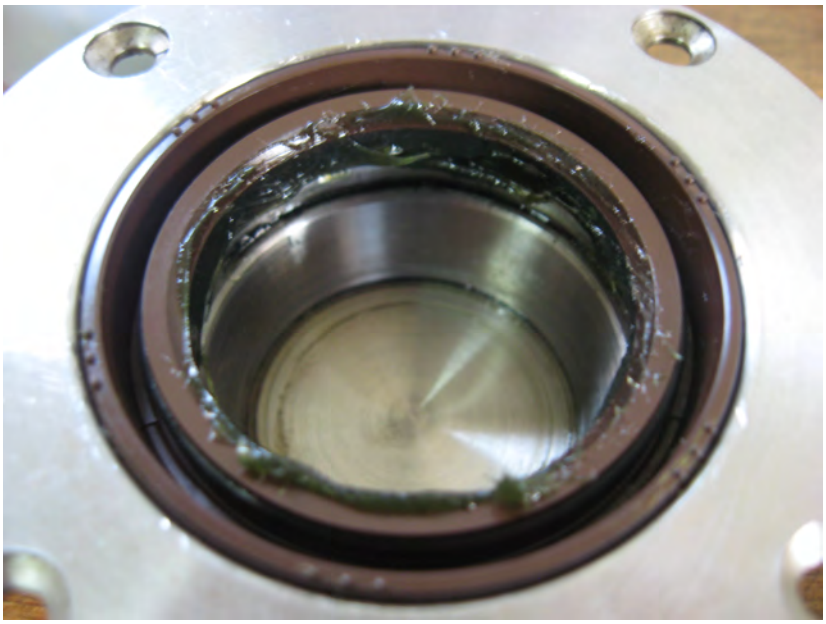

Figure 7: The new seal coated with new grease and mounted in the base. The new seal was able to withstand prolonged ramps without any damage.

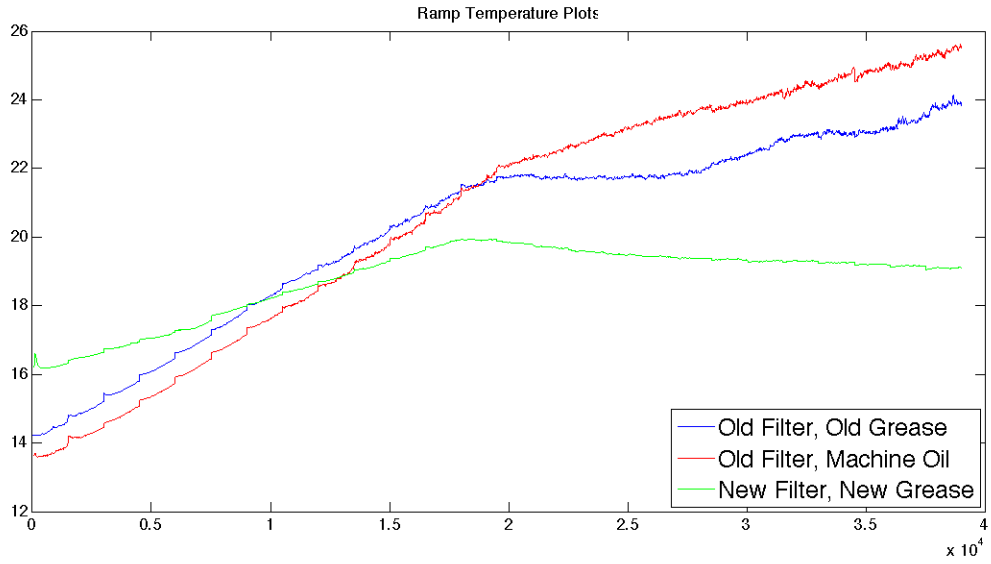

Figure 8: This graph shows the drastic improvement in temperature performance as a result of my mechanical changes. While the total net temperature change for runs of the old setup which were $9.61\,^{\circ}C$ and $11.95\,^{\circ}C$, respectively, the total net change for runs of the new setup was $2.93\,^{\circ}C$, and improved even further during later runs as the apparatus settled.

5 Results

Initial ramps yielded a bifurcation diagram that indicated consistent bifurcation around 1250 rpm.

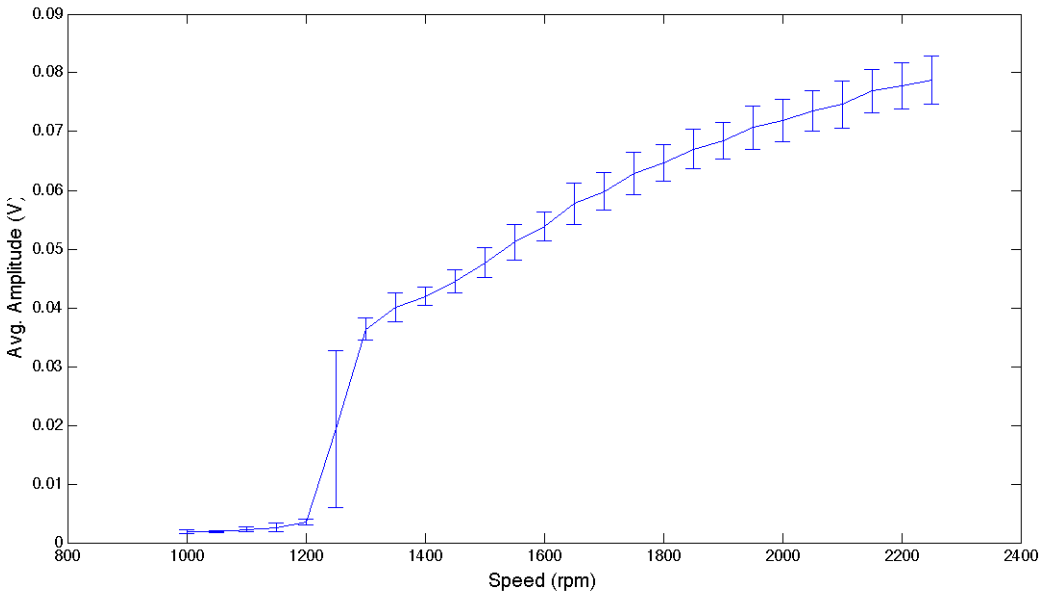

Figure 9: Bifurcation diagram of average wave amplitude vs. rotation speed.

It also agreed with the theoretical prediction from Cristóbal's thesis that the post-bifurcation amplitude should vary with the square root of rotation speed.

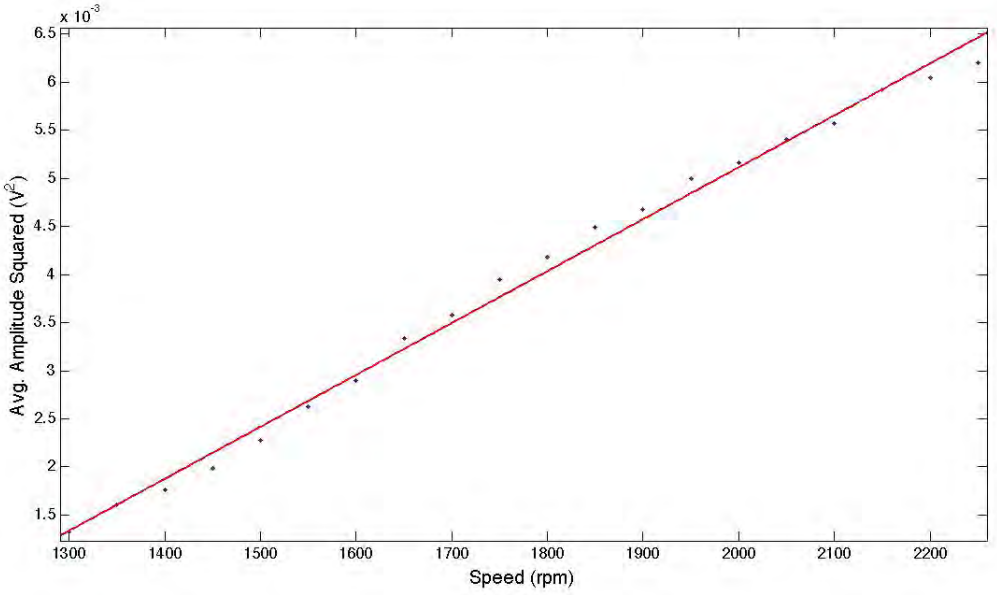

Figure 10: A plot of average amplitude squared vs. rotation speed. Linear correlation with $R^2 = 99.3\%$

At this point in the process of running the experiments, the water began to get cloudy as a result of small amounts of grease escaping from the area above the filter, so I disassembled the system, changed the water to new distilled water, and re-assembled all the components. I then ran a set of ramps over a smaller range of speeds that yielded the following bifurcation diagram.

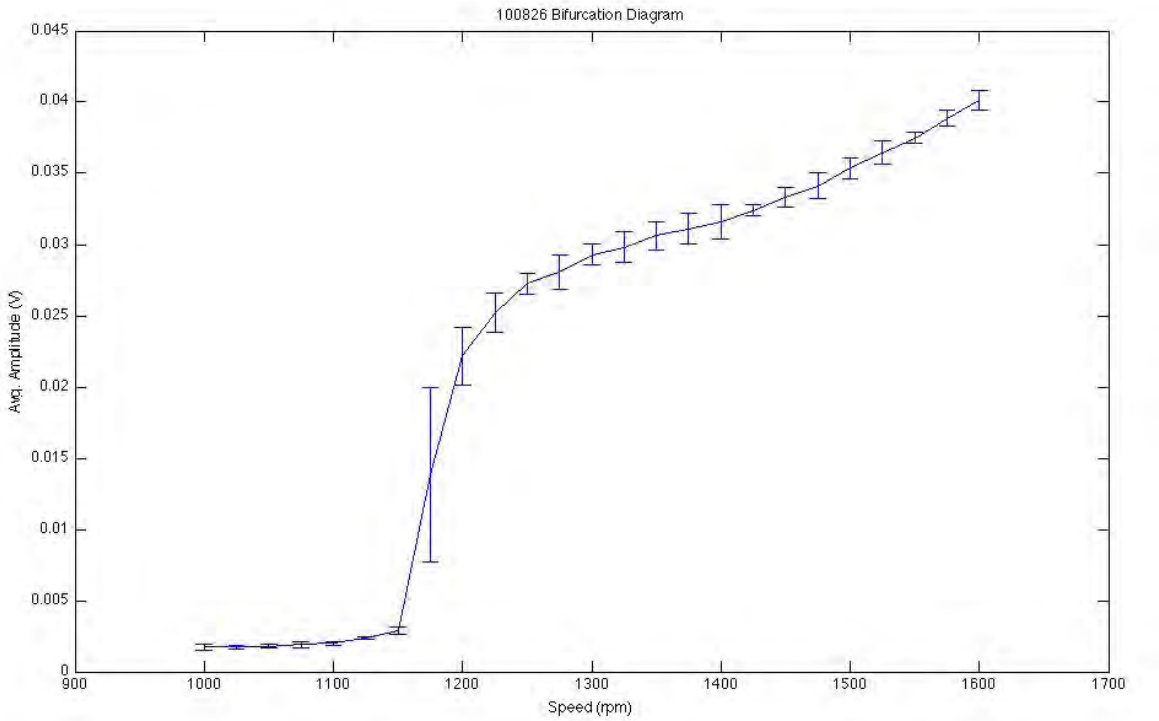

Figure 11: The bifurcation diagram after disassembling and re-assembling the system, showing bifurcation around 1175 rpm.

This ramp indicated bifurcation in a different range, but the critical region of bifurcation was also much wider in the second test. This suggested that either the changed water or the disturbance of the system's mechanical setup influenced the behavior of the instability. To find out what the cause was, I replaced the water again without disturbing the mechanical setup of the system. The results were almost identical, leading me to conclude that the behavior of the bifurcation is heavily dependent on the precise mechanical setup of the system. This is consistent with what Professor Mujica observed in earlier experiments, where he showed that even slight deviations of the spinning rod from vertical caused large changes in the critical region of bifurcation.

6 Conclusions

In addition to fixing the mechanical problems the system had, I was able to identify the critical region of bifurcation to within 50 rpm (after disassembling and re-assembling the system): between 1130 and 1220 rpm. Unfortunately, the system is highly dependent on mechanical alignment, but this problem can be avoided by avoiding disassembling the system. Now that the mechanical problems have been fixed and the apparatus is able to run for long periods without needing maintenance, this should not be a big issue.

Also, I was able to reproduce many of the results found by Cristóbal during his thesis work, including observations of the variation in characteristic modes of the surface.

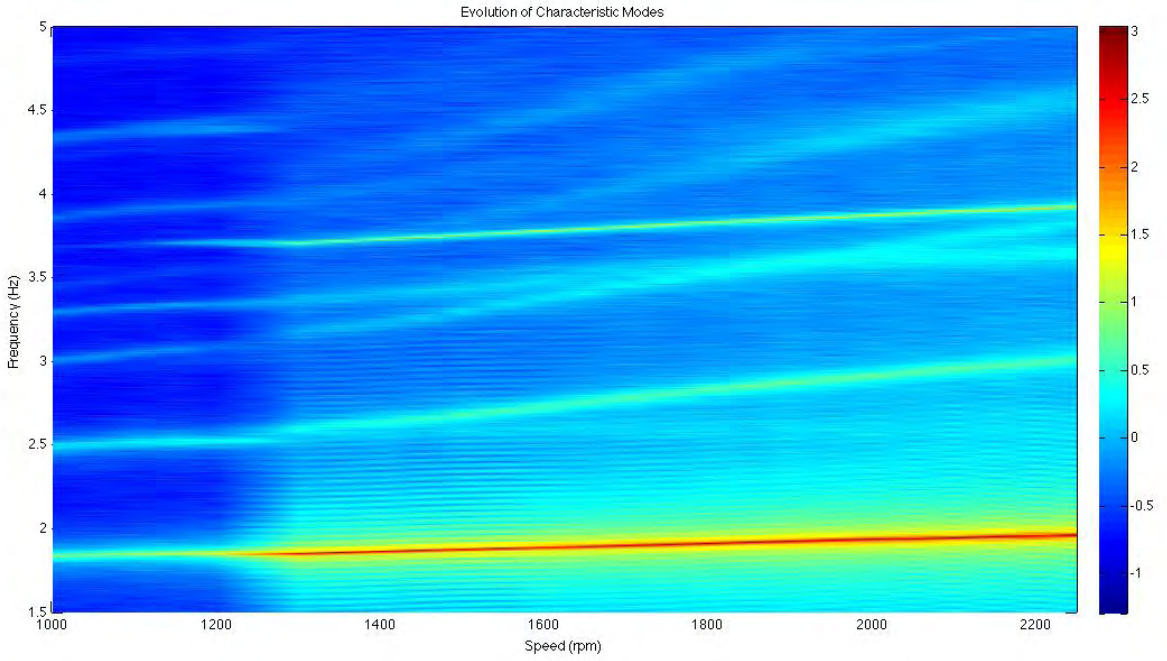

Figure 12: The variation of characteristic modes with rotation speed.

In general, this plot is in qualitiative agreement with that of Cristóbal, including the collision of the third and fourth modes his theory predicted. Though I observed the second mode disappearing and reappearing at a slightly higher frequency in the region of bifurcation, it does not match the mode collision observed by Cristóbal. More experiments will be necessary to get a clearer picture of the cause of bifurcation.

In addition, I ran several very long ramps (approximately eight hours) in an attempt to reproduce the phenomenon observed by Cristóbal of the gravity wave appearing, disappearing, and re-appearing again during a single run. Though I did not reproduce this, I did make some interesting observations near the critical bifurcation frequency.

This data is interesting because it shows that the wave is capable of appearing after long periods of time, indicating that even at speeds below the critical frequency, there is some

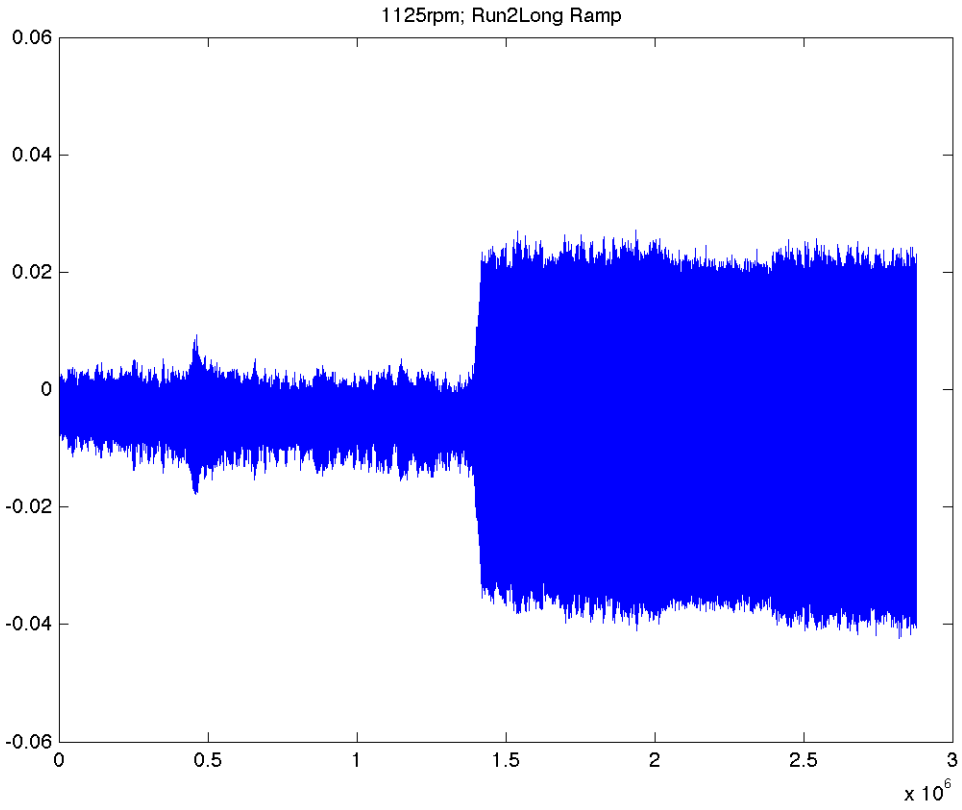

Figure 13: Data from an eight hour ramp, showing the wave appearing after 4 hours of running.

small probability of bifurcation.

7 Topics for Further Investigation

Several aspects of this project would be good to investigate further. For example, though the temperature of the system is largely well-controlled, it is still subject to variations in room temperature. I started working on ideas and implementations of insulating and active cooling systems, but was unable to obtain the necessary parts before leaving. Precise control of the system temperature would be necessary to explore the critical region of bifurcation with consistency.

In addition, I qualititively observed an inverse correlation between the time it takes the wave to appear during rotation and rotation speed, but did not have time to investigate it quantitatively. I will do the analysis on the data I have and submit a secondary report within a few weeks.

References

[1] G.I. Taylor. "Stability of a Viscous Liquid Contained between Two Rotating Cylinders." *Phil. Trans. R. Soc. Lond. A*. 1923. Vol. 223. 289-343.

[2] Reténes DBH. *Católogo General de Medidas*. Published 12/07/2005. Available online at: ¡www.apiro.com/Especificaciones.pdf¿